

Toward Designing Asymmetric Head Gradient Coils for High-Resolution Imaging

VIKTOR VEGH,¹ HECTOR SANCHEZ,² IAN M. BRERETON,¹ STUART CROZIER²

¹ Centre for Magnetic Resonance, University of Queensland, Level 2, Gehrman Laboratories, St. Lucia, Brisbane, Australia

² Electromagnetics and Imaging, School of Information Technology and Electrical Engineering, University of Queensland, St. Lucia, Brisbane, Australia

ABSTRACT: The aim of the research described here is to design head gradient coils using approaches previously developed by the authors. The wave equation method for designing gradient coils is used to design a transverse gradient coil winding on a cylindrical/spherical former. The results are compared with asymmetric cylindrical designs and other well-known head gradient coil designs to establish the quality of the gradient coil winding. Comparisons of field, inductance, torque, and other quality factors are made before conclusions are drawn about the adequacy of such a winding pattern to perform high-resolution imaging of the head. We show that it is possible to generate a robust winding pattern that has good efficiency and produces a sufficiently large imaging volume. © 2007 Wiley Periodicals, Inc. Concepts Magn Reson Part B (Magn Reson Engineering) 31B: 1–11, 2007

KEY WORDS: magnetic resonance imaging; gradient coil design; asymmetric design methodology; insertable; high-resolution imaging

INTRODUCTION

One of the primary goals of current magnetic resonance imaging (MRI) hardware is to perform imaging of the human body at high resolution. Whole-body gradient and radio frequency (RF) coils are conventionally used to obtain images of different body parts. Smaller gradient coils tailored to local anatomical regions offer the potential of higher gradient strengths and, when appropriately combined with local RF coils, produce improved image resolution. A number of strategies have been presented for the design of local gradient coils (1–6). In this article we present

two new designs for head gradient coils and examine each in detail.

The first method presents designs for an asymmetric cylindrical and a dome gradient coil. Leggett et al (5) recently introduced the dome gradient structure. In that work a target field approach was used to generate the final coil winding pattern. A potential difficulty in designing dome structures is the interfacing between the dome and the cylinder, and the manner in which the coil surfaces are restricted to these separate domains. The work in this article aims to remove such boundary limitations and restrictions between the dome and cylinder, and to allow for the wire windings to freely form over these two domains. The second design uses a cylindrical former and uses a flexible design trade-off method to attempt to produce an optimal and realizable design.

In the following sections, two existing methods by the authors for designing head gradient coils are outlined (1, 7). The methods are compared with existing winding patterns using tabulated values, whereby the key factors and variables are compared to assess the quality of

Received 20 September 2006; accepted 6 October 2006

Correspondence to: Viktor Vekh; E-mail: viktor.vegh@cmr.uq.edu.au

Concepts in Magnetic Resonance Part B (Magnetic Resonance Engineering), Vol. 31B(1) 1–11 (2007)

Published online in Wiley InterScience (www.interscience.wiley.com). DOI 10.1002/cmrb.20082

© 2007 Wiley Periodicals, Inc.

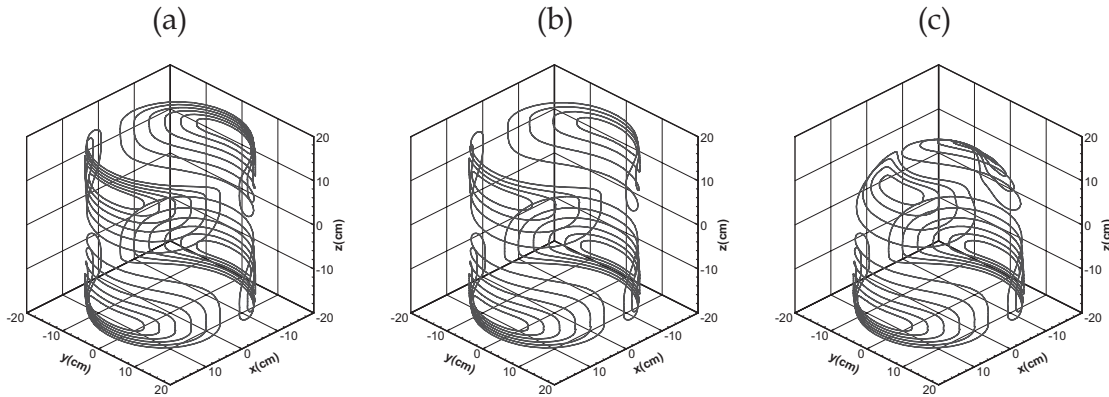


Figure 1 Illustrations of the transverse gradient coil design for the (a) symmetric design, (b) nonequal number of wire windings, and (c) hemispherical end cap.

design. The results section illustrates the winding patterns along with the field distributions as obtained from the winding pattern. Finally, the article draws some conclusions about the designs highlighted here and makes some recommendations regarding designing gradient coils of nonconventional geometries.

METHODS

In this section, two methods are outlined for specialized gradient coil design. The first method was recently published, although it has not been used for an asymmetric design, and the second method, which is an asymmetric cylindrical design based on the target field methodology, is outlined to allow comparison and benchmarking of the results (1, 7). The following sections provide detail of the development of models and methodology used.

Wave Equation Technique (WET)

The previously described wave equation technique (WET) for designing symmetric planar and cylindrical gradient coils has been used in this work to demonstrate the ability of the technique to generate coil windings for high-resolution head imaging (7). The technique has been described in detail by Vegh (7), and here the adaptation of the technique to asymmetric domains is demonstrated.

The wave equation technique is a method of determining the winding patterns based on the solution of a porous media problem governed by the forward propagating wave equation in, for example, liquid phase. The wave front solutions through the porous media become the winding patterns for the gradient coils. The domain on which the waves propagate is

predefined, and the flow is somewhat restricted to two dimensions. The properties of the media through which the liquid flows is changed using the simulated annealing (8) approach, and the final winding path is determined for a number of nonequally spaced wave fronts by the gradient field strength requirements, inductance, and torque.

Figure 1 is an illustrative example of how the symmetric winding patterns can be adopted to the asymmetric design. Figure 1(a) is a depiction of the symmetric cylindrical design, whereby the number of loop windings is six and are the same for each of the quadrants. Figure 1(b) takes account of the fact that the number of windings does not have to be equal, and in this case the windings in the upper two quadrants are reduced to four loops. In Fig. 1(c), the domain upon which the windings are constrained has been altered to allow for curved surfaces and in this case for a hemispherical end cap. The mapping used for converting the cylindrical winding patterns to the hemispherical patterns is

$$\begin{aligned} r &= r_c, \\ \theta &= \cos^{-1}\left(\frac{y_c}{r_c}\right), \\ \phi &= \frac{z_c}{r_c}, \end{aligned} \quad [1]$$

where point (x_c, y_c, z_c) on the cylinder maps to point (x_s, y_s, z_s) on the hemisphere. In Eq. [1], r_c is the radius of the cylindrical shell, θ and ϕ are the transformation mapping angles. In the case of Fig. 1(b), the following transformation mapping was used to reconstruct the winding pattern on the cylinder:

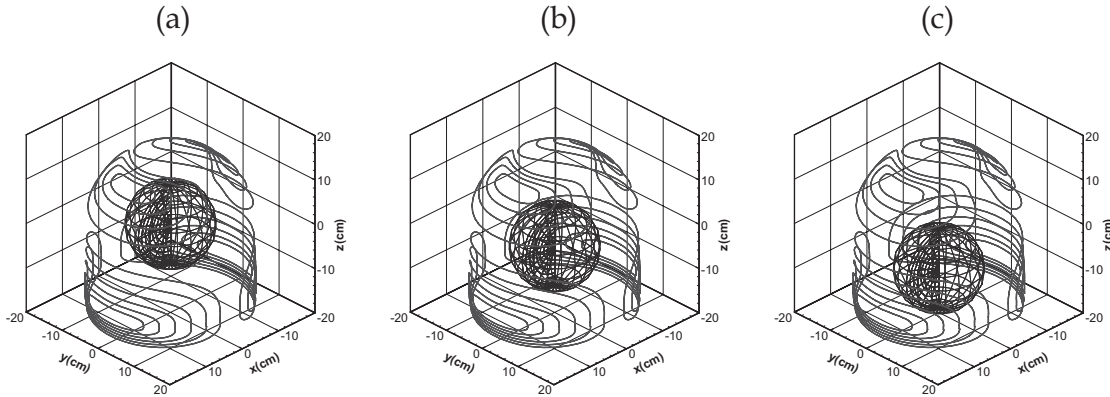


Figure 2 Geometric shift of the imaging volume for a transverse x -gradient coil design (a) 0.0 m, (b) 0.05 m, and (c) 0.1 m.

$$\begin{aligned}
 x_s &= r \cos\left(\theta - \frac{\pi}{2}\right) \sin\left(\phi - \frac{\pi}{2}\right), \\
 y_s &= r \sin\left(\theta - \frac{\pi}{2}\right) \sin\left(\phi - \frac{\pi}{2}\right), \\
 z_s &= r \cos\left(\phi - \frac{\pi}{2}\right). \quad [2]
 \end{aligned}$$

Equation [2] allows for a cylindrical shell to be mapped to a hemispherical shell on which the windings can be calculated. The method is not restricted to this mapping alone but rather it is also possible to map to other domains—for example, ellipsoids and cones.

In asymmetric design methodology, adjustments must be made to the porous media that governs the optimization process using simulated annealing (SA) because the number of windings is no longer the same between the different quadrants and because the domain is not symmetric (8). SA is a stochastic algorithm that has been used for gradient coil design (9). This algorithm can find a global optimum solution with a high probability; however, there is a considerable computational burden in finding an optimum solution because of the high number of evaluations of the objective function. In this work the total number of optimization parameters has been kept to a minimum to ensure that the optimization time is as small as possible.

The quadrants corresponding to the cylindrical section of Fig. 1(c) are governed by one unique density map for which the wave fronts are obtained; a different density map is used in the optimizations to obtain the winding patterns on the hemisphere. That is, rather than using a single density map, as in the case of cylindrical designs, and replicating this map four

times once for each of the quadrants, two distinct density maps are optimized reflecting the manner in which the wires are wound in the cylindrical section and in the hemispherical section.

In the SA algorithm a number of optimization variables are used in determining the final winding pattern of the gradient coil (7). In this work, because the coil windings themselves are not symmetric, it is not desirable to fix the imaging volume to a specific location. It may be that the best gradient performance is required to be achieved at some distance from the edge of the coil. Figure 2 is an illustration of differing positions of the imaging volume. A variable is associated with moving the imaging volume along the z axis, and this variable is limited to a particular feasible range. In the case of the example in Figs. 2(a–c), the range to which movement is constrained equals 10 cm.

Figure 3 depicts the behavior due to another newly introduced variable in the asymmetric design approach. In this case, a variable referred to as the “sliding factor” allows movement between the cylindrical and spherical sections of the design. This variable essentially shifts the windings patterns either in the positive or the negative z -coordinate direction. It is possible to obtain many different types of functions that allow the winding patterns to be shifted along the z axis. A function was sought for which only one variable is required to change the manner in which the z -coordinate dimension shifts the winding along the z axis, to ensure a reduction of the number of free variables and thus minimize the algorithm convergence time.

Figure 4 depicts the different shift functions that can be used to adjust the manner in which the windings overlap between the cylindrical and spherical domains. In Figs. 4(a–c) the solid line corresponds to the upper boundary value of the sliding factor and the

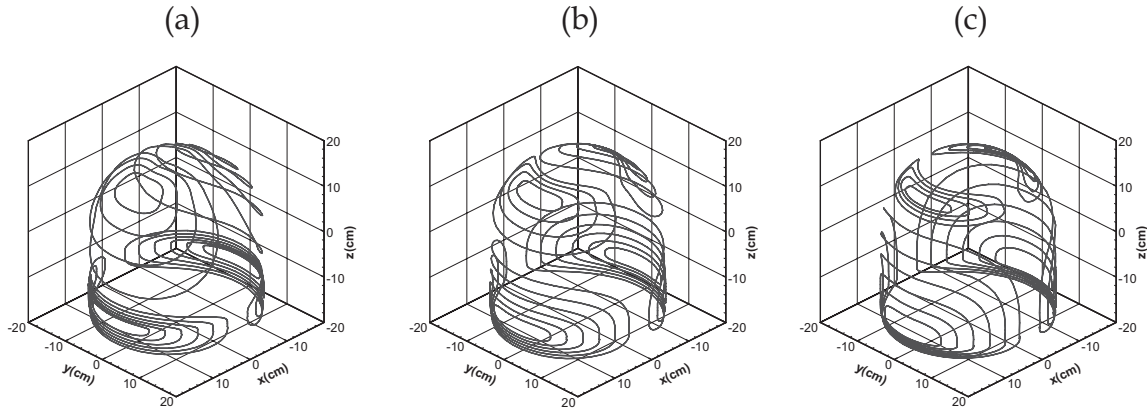


Figure 3 Sliding factor illustrations between the spherical and cylindrical domains for a transverse x -gradient coil design with values (a) 0.5, (b) 1.0, and (c) 1.5.

dashed line is the lower boundary value. Figure 4(a) is the piecewise linear function defined as

$$f(z, \rho) = \begin{cases} z_d \rho \left(1 + \frac{z}{z_d} \right), & z < 0, \\ z_d \rho \left(1 - \frac{z}{z_d} \right), & z > 0. \end{cases} \quad [3]$$

In Eq. [3] ρ is the sliding factor that takes values $-1 < \rho < 1$ for the calculations performed here, and z_d is the coil half dimension in the z direction. Equation [3] provides a linear adjustment on any of the z coordinate values of the wire windings. It is possible to have other functions as well—for example, a quadratic function as elucidated by Fig. 4(b) and expressed in the form

$$f(z, \rho) = z_d \rho \left(1 - \frac{z^2}{z_d^2} \right). \quad [4]$$

Equations [3] and [4] do not satisfy the criteria that $f'(-z_d, \rho) = f'(z_d, \rho) = 0$. Although this is not a necessary condition, in some cases it may be beneficial to have a sliding function that does not alter the values at the boundaries. In such a case, as illustrated in Fig. 4(c), the following function can be used to alter the winding patterns between the different domains:

$$f(z, \rho) = \frac{z_d \rho}{2} \left(1 - \cos\left(\frac{\pi z}{z_d}\right) \right). \quad [5]$$

Given the choice of function as outlined by Eqs. [3], [4], and [5], the z coordinate of each of the wire windings are altered using the following adjustment:

$$z^* \leftarrow z + \nu f(z, \rho), \quad [6]$$

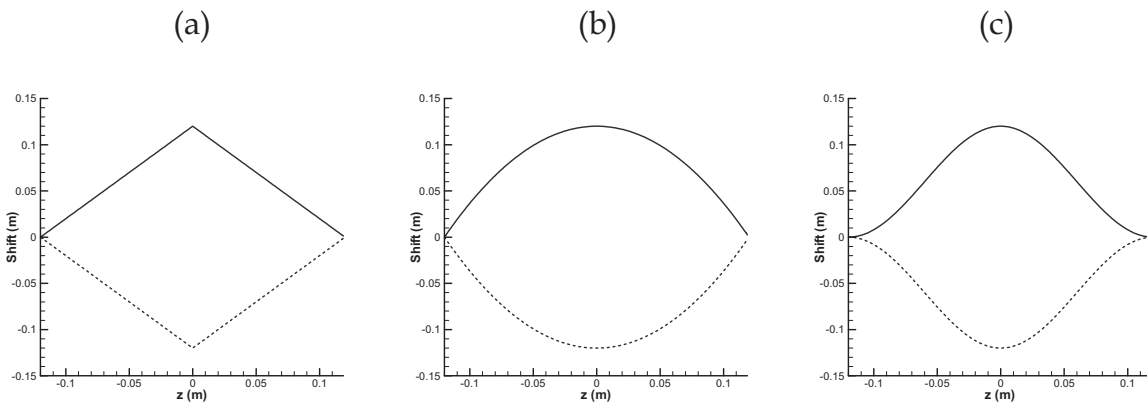


Figure 4 Illustration of the envelopes of the different shift functions used in the simulations; bold lines correspond to $\rho = 1$ and dashed lines correspond to $\rho = -1$, (a) piecewise linear, (b) quadratic, and (c) cosine.

where z^* is the altered z -coordinate value and ν is the magnification factor, which allows the maximum amount of sliding to be altered. In most cases it is not necessary to set this value and therefore $\nu = 1$ in general, but in some special cases it may be necessary to increase or decrease this value according to further constraints. The benefit of the approach defined by Eq. [6] is that only a single optimization variable is required to alter all of the wire windings, hence reducing the overall complexity of the optimization problem.

Overall, the asymmetric wave equation technique is similar to that described in prior work (7), with the addition of a new density map for the two distinct halves and two extra optimization variables, which are the imaging volume shifting parameter and the sliding factor ρ . All other aspects of the methodology remain the same, and no significant changes are necessary to obtain asymmetric winding pattern results.

Relaxed Target Field Approach

The relaxed target field approach (RTFA) has been used in designing multilayer asymmetric and symmetric gradient coils (10). In this method it is assumed that N layers of current density defined as in Sanchez (10) are flowing in concentric cylindrical surfaces of radii ρ_n . The current density distribution is restricted in the axial domain ($0 \leq z \leq 2L_n$), where $2L_n$ is the coil length for the n^{th} layer. The azimuthal component of the current density is expressed as a sum of orthonormal functions multiplied by the unknown amplitudes λ_{nq} , where n corresponds to the layer number and q is the number representing the mode of oscillation for the current density function (10).

The magnetic field and gradient components are calculated using Biot-Savart's law, which is sufficiently flexible to allow for expansions in the method for arbitrary geometrical surfaces. The magnetic field gradient condition at a point t located within the volume of imaging is expressed in the form of a relaxed linear constraint as follows:

$$|G_{x_t} - G_0| \leq \varepsilon G_0, \quad t = 1, 2, \dots, T, \quad [7]$$

where G_{x_t} is the x -gradient field contribution at the point t of each node of the axial component of the current density oscillating in each surface layer n . T is the number of target points in the target field region, G_0 is the target gradient strength specified at the target point t measured in (T/m), and ε is the relaxation factor. The relaxation factor ε in Eq. [7] allows for control over the desired target gradient uniformity, and at the same time relaxes the boundary conditions in the volume of inter-

est. Essentially, this factor can increase the solution space and, as a consequence of changing this factor, it is possible to obtain improved configurations with better credentials. In this method the stored magnetic energy is expressed as a quadratic function of the unknown current density amplitude λ_{nq} as follows:

$$E = \sum_{n=1}^N \sum_{q=1}^Q \sum_{n'=1}^N \sum_{q'=1}^Q E_{nqn'q'} \cdot \lambda_{nq} \lambda_{n'q'}. \quad [8]$$

The matrix $E_{nqn'q'}$ contains the self and all of the mutual magnetic energy interactions among all axial modes of the current density flowing in the cylindrical surfaces. The resultant torque and force are expressed as a linear function of the unknown amplitude. This means that the magnetic field, torque, and force conditions can be included as linear constraints in a quadratic programming optimization algorithm by minimizing:

$$\frac{1}{G_0^2 \rho_1^5} \sum_{n=1}^N \sum_{q=1}^Q \sum_{n'=1}^N \sum_{q'=1}^Q E_{nqn'q'} \cdot \lambda_{nq} \lambda_{n'q'}. \quad [9]$$

Equation [9] is subjected to the following constraints:

$$\sum_{n=1}^N \sum_{q=1}^Q G_{x_{qn}} \cdot \lambda_{nq} \leq G_0(1 + \varepsilon), \quad t = 1, 2, \dots, T;$$

$$- \sum_{n=1}^N \sum_{q=1}^Q G_{x_{qn}} \cdot \lambda_{nq} \leq -G_0(1 - \varepsilon), \quad t = 1, 2, \dots, T;$$

$$\left| \sum_{n=1}^N \sum_{q=1}^Q (B_{z_{qn}} \cdot \lambda_{nq}) \right| \leq B_{z_t}^{\text{shield}}, \quad t = T + 1, 2, \dots,$$

$T + P;$

$$\left| \sum_{n=1}^N \sum_{q=1}^Q (T_{y_{nq}} \cdot \lambda_{nq}) \right| \leq T_{y0},$$

$$\left| \sum_{n=1}^N \sum_{q=1}^Q (F_{x_{nq}} \cdot \lambda_{nq}) \right| \leq F_{x0}. \quad [10]$$

Table 1 Technique Specific Parameters as Obtained Using Computational Techniques; (a) RTFA, (b) WEM Applied to the Cylinder, (c) WEM Applied to the Modified Domain without Imaging Volume Shifting and (d) WEM Applied to the Modified Domain with Imaging Volume Shifting

Description	(a)—Figure 5	(b)—Figure 6	(c)—Figure 7	(d)—Figure 8
<i>Type</i>	<i>Cylindrical</i>	<i>Cylindrical</i>	<i>Tapered end</i>	<i>Tapered end</i>
# primary windings	12	12	5 + 7 = 12	8 + 4 = 12
# shield windings	3	3	2 + 3 = 5	3 + 2 = 5
Primary winding diameter (cm)	35	35	35	35
Shield winding diameter (cm)	55	55	55	55
Length of coil winding (cm)	56	56	46	44
Imaging volume centre from edge (cm)	13	14	22	13
Inductance [L] (μH)	56	42	23	27
Resistance (Ω)	0.259	0.205	0.213	0.226
Torque ($NmA^{-1}T^{-1}$)	0.563	0.580	0.0357	0.302
Efficiency [α] ($Tm^{-1}A^{-1} \times 10^{-3}$)	0.115	0.0750	0.127	0.110
Switching efficiency [η]	0.01427	0.008100	0.04211	0.02698
$\alpha^2/L (\times 10^{-3})$	0.236	0.134	0.701	0.448

The algorithm searches for the minimum current density amplitudes λ_{nq} that maximize the magnetic energy and at the same time fulfill the relaxed linear gradient field conditions under constrained values of torque (T_{y0}) and force (F_{x0}) and the axial component of magnetic field $B_{z_i}^{\text{shield}}$ specified at P points located at the cylindrical surface of radius ρ_s^{fringe} and axial length L_s^{fringe} . In this case the superscript *fringe* refers to dimensions where the fringe field error is minimized.

RESULTS

In this section a number of methods were used to compute results for different transverse gradient coil arrangements with the aim to obtain high-resolution imaging of the brain. Coil structures were generated for RTFA and WET and these are compared.

All of the results were generated in such a manner as to obtain at least an imaging volume that is spherical and has a diameter no less than 15 cm at the 5% contour line. Due to the asymmetric nature of the windings, it was also necessary to numerically compute the torque exerted on the coils. The inductance of the coil windings and their efficiency were also determined and these values are used in the comparisons to establish the quality of the different coils.

In previous work a so-called “switching efficiency” was used to obtain a figure of merit for comparison of different coils (11). The figure of merit referred to as η is calculated using the following formulation:

$$\eta = \frac{\alpha^2 d^5}{\mu_0 L}. \quad [11]$$

In Eq. [11] d is the diameter of the spherical imaging volume, $\alpha (Tm^{-1}A^{-1})$ is the efficiency, and $L(H)$ is the inductance, as quoted in Table 1. From the switching efficiency a figure of merit can also be obtained by removing the constants, in this case d and μ_0 to have an expression as

$$\frac{\alpha^2}{L}. \quad [12]$$

Equation [12] is the generalized figure of merit for a coil with a particular efficiency and inductance. In the table, the number of primary and active shield windings is also stated, along with the torque for the particular coil as obtained by the method of choice. The resistance of the coil as stated in the table is obtained for a copper wire with a 1.5 mm \times 1.5 mm cross section. The windings were restricted to have at least a 4 mm separation between any two adjacent wire paths for all of the results illustrated here.

Figure 5 is an illustration of results obtained using RTFA. Figures 5(a–c) are the primary, shield, and combination of primary and shield windings, respectively. Figure 5(d) illustrates the location and size of the region in which the axial component of the magnetic field values have been calculated. Figure 5(e) depicts the gradient in the x -coordinate direction of the axial field, and Fig. 5(f) the relative error in the x -gradient field plotted using 5% contour line intervals. Figures 5(g–i) are depictions of the relative error in the region of interest when different slices through the center of the sphere have been taken where a fixed 15-cm diameter dashed ring indicates the imaging volume.

Figure 6 is a set of plots highlighting the results obtained when WET was used to simulate the results

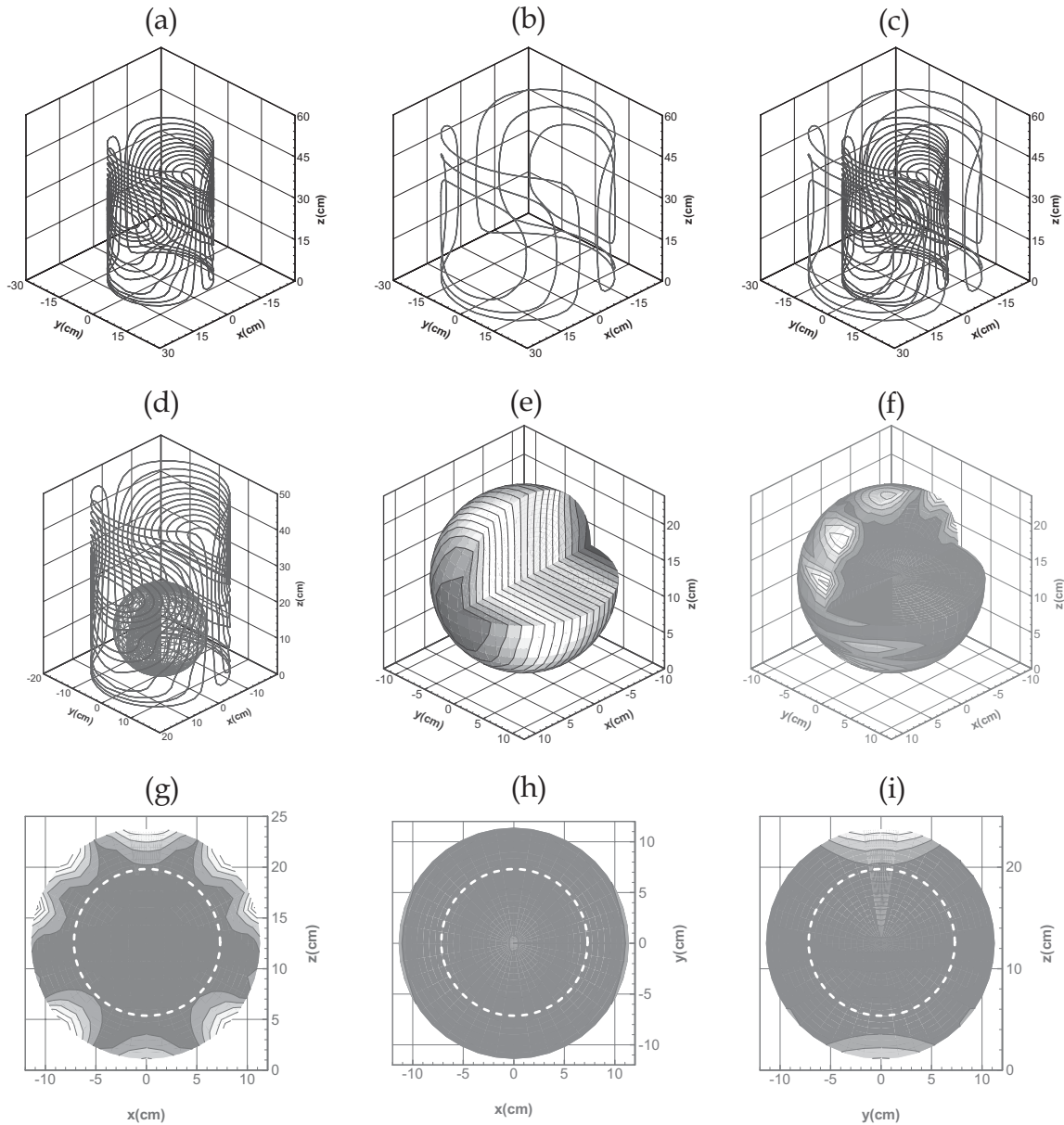


Figure 5 Results of the transverse gradient coil windings using RTFA. Illustration of the (a) primary winding pattern, (b) shield winding pattern, (c) combined winding pattern, (d) volume in which the field values are computed, (e) magnetic field, (f) error in the gradient field using 5% contour lines, (g) xz -plane plot of the error, (h) xy -plane plot of the error, and (i) yz -plane plot of the error.

of RTFA. In this case, the aim was to match the results obtained using RTFA with WET. It is clear from Figs. 5 and 6 that the results are different and, in particular, columns (a) and (b) of Table 1 clearly identify the differences in the winding patterns of the different methods. The number of primary and shield windings were chosen to be the same for Table 1(a) and 1(b), and in the case of WET with the tapered end, only the number of primary windings was chosen to be fixed. The constraints of optimization in WET for

Table 1(b) were set to values that would provide results for which the torque was in the range of the torque obtained using RTFA (see Table 1(b)).

Figure 7 is an implementation of WET for which one end of the cylinder has been tapered. In this case the imaging volume has been allowed to shift in the z -coordinate direction. The aim of the optimization strategy was to obtain an imaging volume that is at least 15 cm in diameter, and at the same time, the wire winding has been optimized to have minimal torque

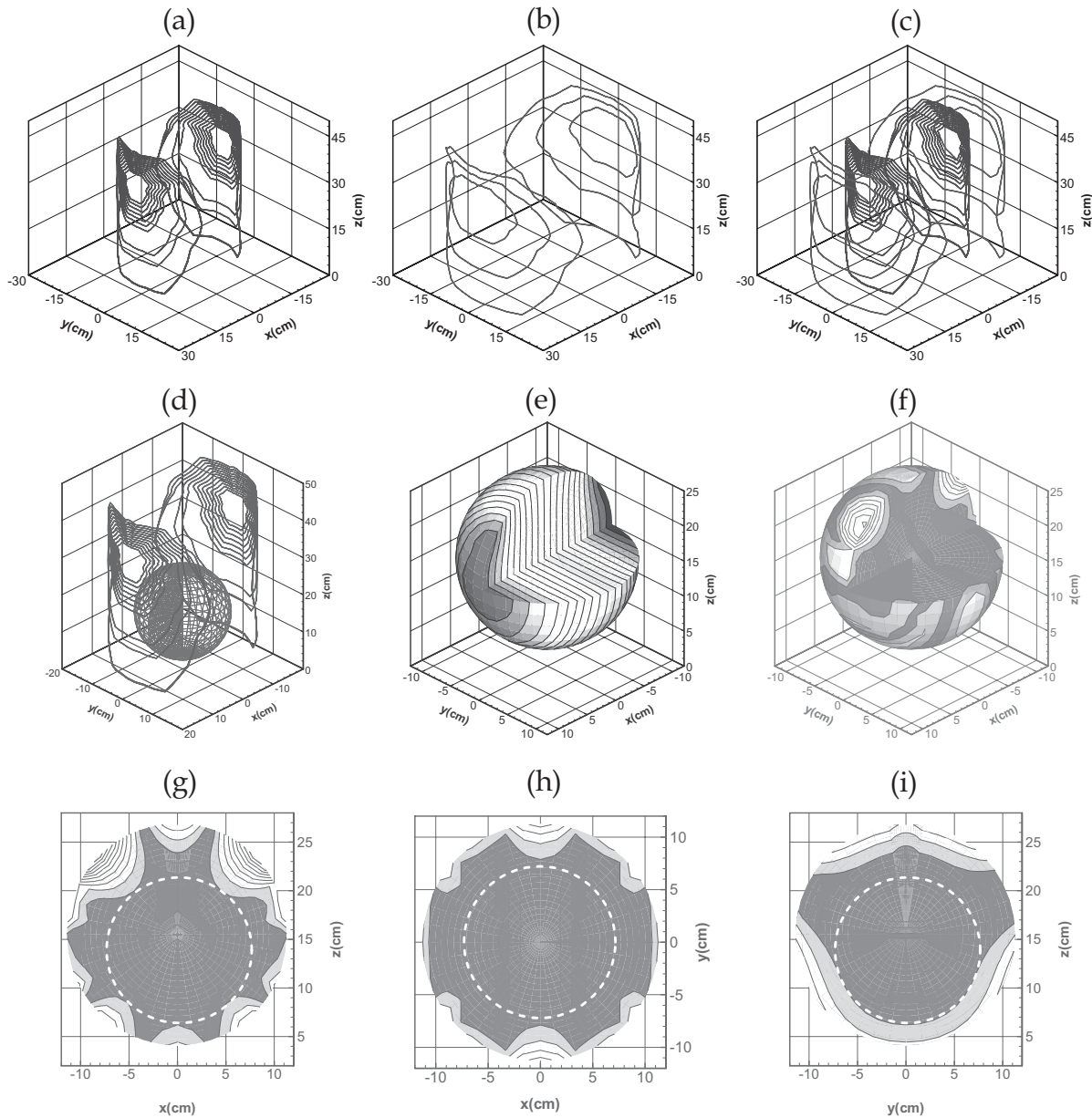


Figure 6 Results of the transverse gradient coil windings using WET for the cylindrical case. Illustration of the (a) primary winding pattern, (b) shield winding pattern, (c) combined winding pattern, (d) volume in which the field values are computed, (e) magnetic field, (f) error in the gradient field using 5% contour lines, (g) xz -plane plot of the error, (h) xy -plane plot of the error, and (i) yz -plane plot of the error.

given the imaging volume constraints. From Table 1(c) it can be seen that for this design, the torque is considerably reduced, although at the cost of pushing the imaging volume away from the $z = 0$ plane.

Although in Fig. 7 the torque is minimal and the switching efficiency is high, it may not be a good choice to use such a winding pattern in practice, since the center of the imaging volume is located at a distance of 22 cm from the edge of the coil winding.

This is to say that no useful images can be obtained in the first 14.5 cm of this particular coil design. For this reason, in Fig. 8 the shifting parameter was removed and the imaging volume was constrained to be at a distance identical to that of RTFA. The pattern and field values computed when the imaging volume is not allowed to move is without torque optimization and the results are elucidated in Fig. 8 and Table 1(d). As before, the size of the imaging volume was con-

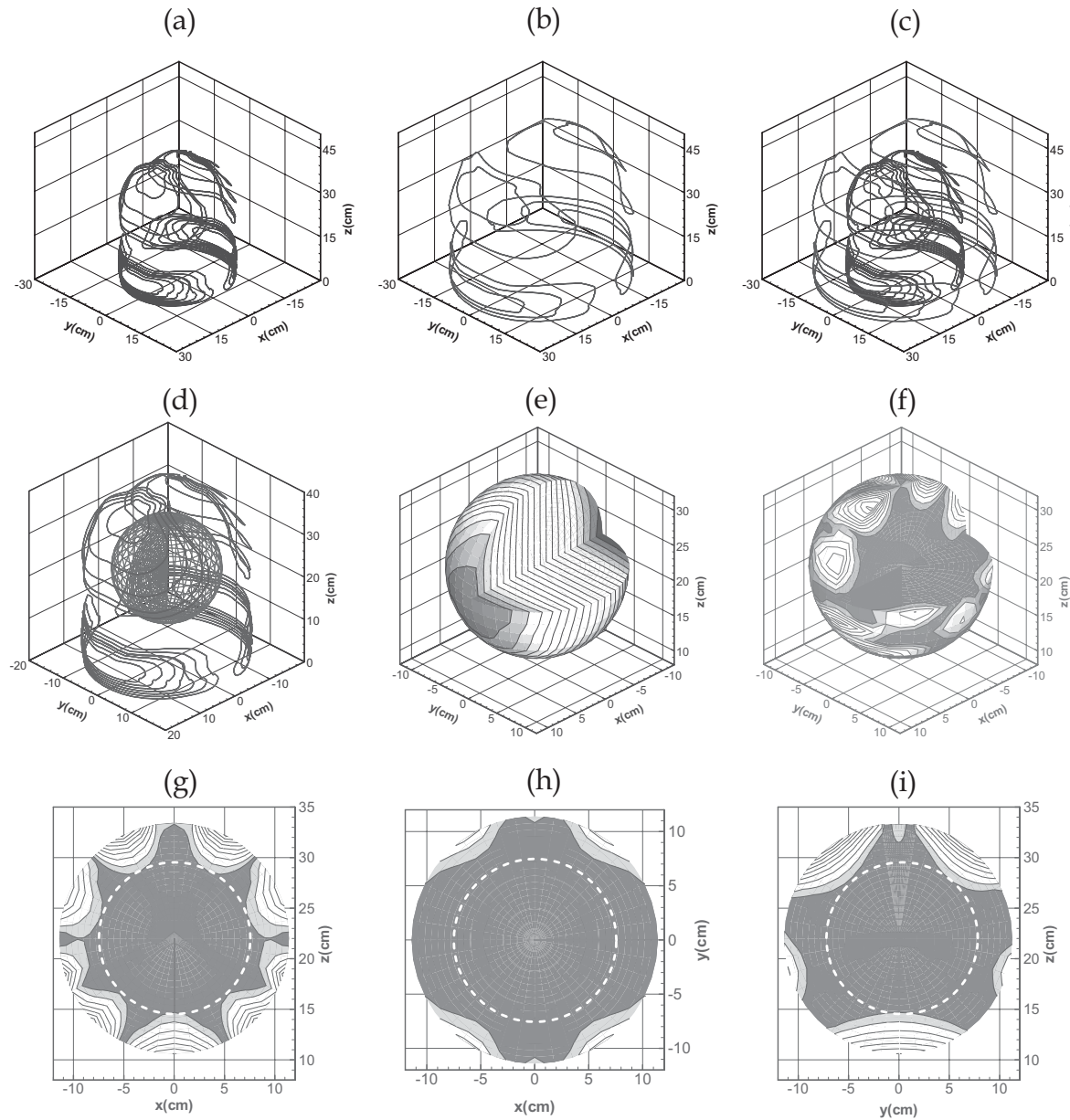


Figure 7 Results of the transverse gradient coil windings using WET with imaging volume shifting for the tapered end case. Illustration of the (a) primary winding pattern, (b) shield winding pattern, (c) combined winding pattern, (d) volume in which the field values are computed, (e) magnetic field, (f) error in the gradient field using 5% contour lines, (g) xz -plane plot of the error, (h) xy -plane plot of the error, and (i) yz -plane plot of the error.

sidered to be at least 15 cm in diameter, and the primary windings were constrained to a total of 12 wire loops, to be somewhat consistent with all the other results outlined in this article.

Generally, when the value of the torque is incorporated into the computation of the objective function for the optimization strategy, the imaging volume is shifted toward the center of the coil. This observation makes sense because in classical symmetric cylindrical

designs the torque is zero due to the fact that the imaging volume is located at the isocenter of the gradient coils. For this reason, when designing coils, it may not be appropriate to allow the imaging volume to shift entirely in the z -coordinate direction, but rather a limit is set on this parameter and the maximum disposition is stated as opposed to allowing complete free movement of the imaging region.

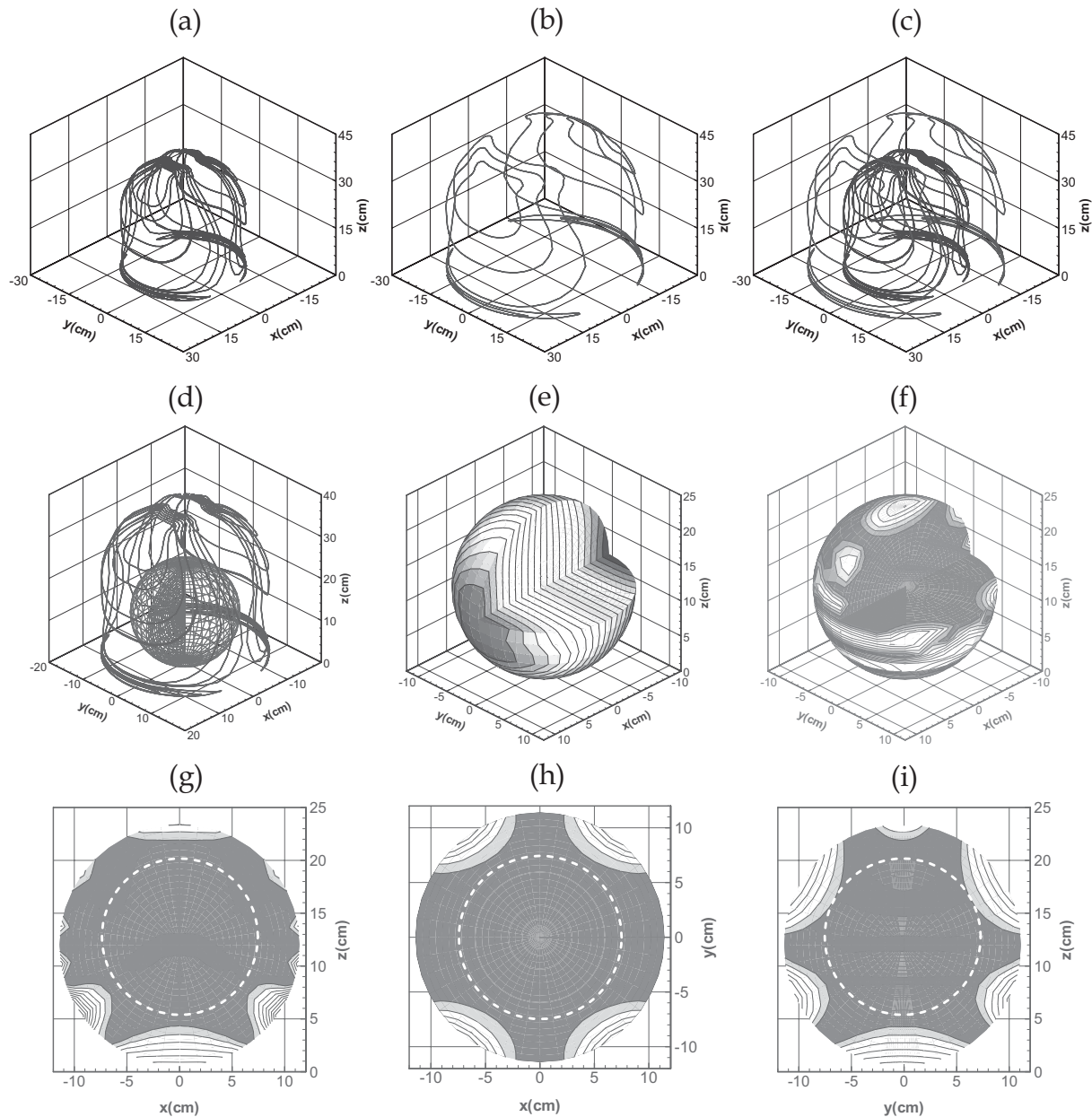


Figure 8 Results of the transverse gradient coil windings using WET without imaging volume shifting for the tapered end case. Illustration of the (a) primary winding pattern, (b) shield winding pattern, (c) combined winding pattern, (d) volume in which the field values are computed, (e) magnetic field, (f) error in the gradient field using 5% contour lines, (g) xz -plane plot of the error, (h) xy -plane plot of the error, and (i) yz -plane plot of the error.

The results of Fig. 8 and Table 1(d) support the notion that it is possible to obtain coil windings with low inductance for which the imaging volume is close to the edge of the coil pattern. It is clear that the torque is considerably reduced and the switching efficiency is high. A number of tests were conducted for a scenario in which the imaging volume is fixed to a particular location. Here only one result is illustrated,

although it is possible to obtain larger imaging volumes at the cost of increasing the torque, or have a winding pattern with lower torque at the cost of decreasing the imaging volume. The specified requirements of the design were met when the imaging volume diameter was 15 cm and only these results are depicted.

We note that the coils for which the ends have been tapered are shorter than the coils that are wound on

cylindrical surfaces (see Table 1). This means that the overall length of the wire required to wind the coil is also reduced, and for this reason manufacturing costs are likely to be cheaper in the case of the tapered windings. From Table 1 it is also evident that the switching efficiency and torque for such coil designs are traded off against one another. It is desirable to have low torque and at the same time a high switching efficiency. It is believed that a sufficient trade-off has been achieved in the case of Table 1(d). In this case, the torque is approximately half that of the cylindrical designs with nearly double the switching efficiency when compared with Table 1(a) and 1(b) entries. The final row of Table 1 represents the figure of merit, which confirms the same findings as for the switching efficiency. Table 1(d) is clearly the most efficient coil design for a given fixed imaging volume size. Although the amount of wire required for this design is greater than that of Table 1(b) and 1(c), it is still less than that of RTFA. This assertion can be deduced from the value of the resistance for the different coils, which is also an indication of the possible cooling requirements.

CONCLUSIONS

In this work, a number of approaches have been investigated to assess the manner in which specialty high-resolution gradient coils can be wound to enable imaging of the brain. RTFA was used to obtain an asymmetric transverse actively shielded gradient coil winding mounted on a cylindrical surface. Results obtained using WET were compared with the RTFA and a number of key parameters were evaluated—for example, efficiency, size, torque, switching efficiency, and a figure of merit relating the efficiency to the inductance of the coil. It was shown that it is possible to obtain good-quality transverse gradient coils using the techniques outlined in this work. These designs produce good efficiency and low technique-dependent torque, and they provide imaging volumes of large diameter when compared with the inner diameter of the gradient coils.

Overall, it was shown that using WET it is possible to numerically obtain a transverse gradient coil winding pattern that has low inductance, high efficiency, low torque, large imaging volume that is located close to the edge of the gradient coil for accessibility, and a good figure of merit. It was also shown that such a coil is smaller in size than that obtained using RTFA. The results show that the wave equation technique with tapered end cap for the coil winding can obtain

results with the lowest torque and highest efficiency for a predefined imaging volume size.

Using a strategy such as WET, one may obtain more flexible wire patterns for gradient coils as opposed to, for example, the target field method, whereby basis functions are required in the appropriate coordinate system. WET is not constrained to any geometry or any coordinate system and can therefore be easily adapted to many different gradient coil design applications.

The coil windings for the wave equation technique have been obtained using the simulated annealing methodology. Future work will see the investigation of different optimization strategies to generate wire winding patterns, for which the computational times and results will be compared with one another to determine an optimization approach that provides the best results in the least amount of time.

REFERENCES

1. Crozier S, Luescher K, Hinds G, Roffmann WU, Doddrell DM. 1999. Designs for an asymmetric gradient set and a compact superconducting magnet for neural magnetic resonance imaging. *Rev Sci Instrum* 70:4062–4066.
2. Abduljalil AM, Aletras AH, Robitaille P-ML. 1994. Torque free asymmetric gradient coils for echo planar imaging. *Magn Reson Med* 31:450–453.
3. Alsop DC, Connick TJ. 1996. Optimization of torque-balanced asymmetric head gradient coils. *Magn Reson Med* 35:875–886.
4. Tomasi D, Xavier RF, Foerster B, Panepucci H, Tannus A, Vidoto EL. 2002. Asymmetric gradient coil for head imaging. *Magn Reson Med* 48:707–714.
5. Leggett J, Green D, Bowtell R. 2006. Insert dome gradient coils for brain imaging. *Proc Int Soc Magn Reson Med* 14.
6. Chronik BA, Alejski A, Rutt BK. 2000. Design and fabrication of a three-axis edge ROU head and neck gradient coil. *Magn Reson Med* 44:955–963.
7. Vegh V, Zhao H, Brereton IM, Galloway GJ, Doddrell DM. 2006. A wave equation technique for designing compact gradient coils. *Concepts Magn Reson B* 29B(2):62–74.
8. van Laarhoven PJM. 1987. *Simulated annealing: theory and applications*. Dordrecht: Reidel.
9. Crozier S, Doddrell DM. 1993. Gradient-coil design by simulated annealing. *J Magn Reson* 103:354–357.
10. Sanchez H, Liu F, Trakic A, Crozier S. 2006. A simple relationship for high efficiency-gradient uniformity trade-offs in multi-layer asymmetric gradient coils for MRI. *IEEE Trans Magn*, in press.
11. Vegh V, Zhao H, Doddrell DM, Brereton IM, Galloway GJ. 2005. The design of planar gradient coils part 2: a weighted superposition method. *Concepts Magn Reson* 27B:25–33.